

Electric-type Stern-Gerlach effect

Jiang-Lin Zhou(周蒋麟), Zou-Chen Fu(傅邹晨), Choo Hiap Oh(胡祖协), and Jing-Ling Chen(陈景灵)
Citation: Chin. Phys. B, 2026, 35 (**1**): 010302. DOI: 10.1088/1674-1056/ae111e
http://cpb.iphy.ac.cn; http://iopscience.iop.org/cpb

What follows is a list of articles you may be interested in

Impact of surface passivation on the electrical stability of strained germanium devices

Zong-Hu Li(李宗祜), Mao-Lin Wang(王茂粼), Zhen-Zhen Kong(孔真真), Gui-Lei Wang(王桂磊), Yuan Kang(康原), Yong-Qiang Xu(徐永强), Rui Wu(吴睿), Tian-Yue Hao(郝天岳), Ze-Cheng Wei(魏泽成), Bao-Chuan Wang(王保传), Hai-Ou Li(李海欧), Gang Cao(曹刚), and Guo-Ping Guo(郭国平)
Chin. Phys. B, 2025, 34 (**9**): 090305. DOI: 10.1088/1674-1056/add4de

Analytical solution to incident angle quasi-phase-matching engineering for second harmonic generation in a periodic-poled lithium niobate crystal

Li-Hong Hong(洪丽红), Ya-Ting Qiu(邱雅婷), Xiao-Ni Li(李晓霓), Bao-Qin Chen(陈宝琴), and Zhi-Yuan Li(李志远)
Chin. Phys. B, 2024, 33 (**2**): 020301. DOI: 10.1088/1674-1056/ad0628

Rigorous solution to second harmonic generation considering transmission and reflection of light at air-crystal interface

Ya-Ting Qiu(邱雅婷), Li-Hong Hong(洪丽红), and Zhi-Yuan Li(李志远)
Chin. Phys. B, 2023, 32 (**5**): 050301. DOI: 10.1088/1674-1056/ac9fc5

Quantum routing of few photons using a nonlinear cavity coupled to two chiral waveguides

Jian-Shuang Liu(刘建双), Ya Yang(杨亚), Jing Lu(卢竞), and Lan Zhou(周兰)
Chin. Phys. B, 2022, 31 (**11**): 110301. DOI: 10.1088/1674-1056/ac7f8f

Analytical model of tilted driver-pickup coils for eddy current nondestructive evaluation

Bing-Hua Cao(曹丙花), Chao Li(李超), Meng-Bao Fan(范孟豹), Bo Ye(叶波), Gui-Yun Tian(田贵云)
Chin. Phys. B, 2018, 27 (**3**): 030301. DOI: 10.1088/1674-1056/27/3/030301

RAPID COMMUNICATION

Electric-type Stern–Gerlach effect

Jiang-Lin Zhou(周蒋麟)[1], Zou-Chen Fu(傅邹晨)[1], Choo Hiap Oh(胡祖协)[2], and Jing-Ling Chen(陈景灵)[3,†]

[1] *School of Physics, Nankai University, Tianjin* 300071, *China*
[2] *Centre for Quantum Technologies and Department of Physics, National University of Singapore* 117543, *Singapore*
[3] *Theoretical Physics Division, Chern Institute of Mathematics, Nankai University, Tianjin* 300071, *China*

(Received 2 September 2025; revised manuscript received 29 September 2025; accepted manuscript online 9 October 2025)

The Stern–Gerlach (SG) experiment is a fundamental experiment for revealing the existence of "spin". In this experiment, beams of silver atoms are sent through inhomogeneous magnetic fields to observe their deflection. Thus, the conventional SG experiment can be viewed as a magnetic-type spin effect. In this work, we successfully generalize the SG effect from magnetic-type to electric-type by solving Dirac's equation with a potential barrier, revealing an extraordinary spin effect. Beams of Dirac particles can be regarded as matter waves. Based on Dirac's equation, we obtain the explicit forms of the incident, reflected, and transmitted waves. The electric-type SG effect shows that the reflected and transmitted waves can exhibit notable spatial shifts, which depend on the spin direction and the incident angle of the wave. The electric-type SG effect has potential applications for separating Dirac particles with different spin directions and for estimating the spin direction of Dirac particles. Some discussions related to the interaction between spin and the electric field are also presented.

Keywords: Dirac's electron, reflection and transmission, spin, Stern–Gerlach experiment, electric-type Stern–Gerlach effect

PACS: 03.65.Pm, 03.75.–b, 03.65.NK

DOI: 10.1088/1674-1056/ae111e **CSTR:** 32038.14.CPB.ae111e

1. Introduction

The Stern–Gerlach (SG) experiment is undoubtedly one of the fundamental experiments in quantum physics.[1] This experiment was performed in 1922 at the University of Frankfurt, where beams of silver atoms were sent through inhomogeneous magnetic fields to observe their deflection. The outcome of the SG experiment firmly confirmed Niels Bohr's previous conjecture, namely, that these atoms have quantized magnetic moments which can take two values. Later, Pauli introduced a "two-valued" degree of freedom for electrons without suggesting a physical interpretation. In 1925, Uhlenbeck and Goudsmit[2,3] boldly proposed the hypothesis of *electronic spin*, due to which the famous SG experiment, together with other experiments related to the quantized magnetic moment, could eventually achieve satisfactory interpretations.

In 1928, Dirac developed the theory of relativistic quantum mechanics by formulating a fundamental equation — Dirac's equation.[4] Based on this equation, electronic spin is no longer a hypothesis but a natural corollary of relativistic quantum theory for electrons. As a cornerstone equation, Dirac's equation not only provides the correct interpretation for existing relativistic quantum effects, such as the SG effect mentioned above, but also stimulates novel predictions, such as the existence of anti-particles.

Dirac's equation for an electron with vector potential $\mathcal{A}$ and scalar potential Φ is given by $H|\Psi\rangle = E|\Psi\rangle$, where E is the energy, $|\Psi\rangle$ is the wave-function (i.e., matter wave), and Dirac's Hamiltonian is given by[5]

$$H = c\boldsymbol{\alpha}\cdot\boldsymbol{\Pi} + \beta mc^2 + q\Phi, \tag{1}$$

where $\boldsymbol{\alpha}$ and β are 4×4 Dirac matrices, $\boldsymbol{\Pi} = \boldsymbol{p} - (q/c)\mathcal{A}$ is the canonical momentum, c is the speed of light in vacuum, and $\boldsymbol{p}$, m, and q are the linear momentum, mass, and electric charge, respectively. Dirac's equation naturally interprets the above SG effect. Explicitly, by choosing $\Phi = 0$ and an appropriate $\mathcal{A}$, an inhomogeneous magnetic field along the z-direction, $\mathcal{B} = \boldsymbol{\nabla}\times\mathcal{A} \simeq B(\boldsymbol{r})\,e_z$, is obtained. In the non-relativistic limit, Dirac's Hamiltonian reduces to Pauli's Hamiltonian $H_{\rm Pauli} = \boldsymbol{\Pi}^2/(2m) + \boldsymbol{\mu}\cdot\mathcal{B}$, with $\boldsymbol{\mu} = -[q\hbar/(2mc)]\boldsymbol{\sigma}$ the magnetic moment vector, $\hbar$ Planck's constant, and $\boldsymbol{\sigma} = (\sigma_x, \sigma_y, \sigma_z)$ the vector of Pauli matrices.[6] Because (i) the force acting on the moment $\boldsymbol{\mu}$ reads $\boldsymbol{F} = \boldsymbol{\nabla}(\boldsymbol{\mu}\cdot\mathcal{B}) \simeq \mu_z(\partial B(\boldsymbol{r})/\partial z)e_z$, and (ii) the Pauli matrix σ_z takes two possible values (i.e., ± 1), silver atoms with positive/negative μ_z are deflected upwards/downwards, thus successfully explaining the SG experiment.

If one re-examines the SG experiment from the perspective of Dirac's equation, it is evident that the SG experiment

†Corresponding author. E-mail: chenjl@nankai.edu.cn

© 2026 Chinese Physical Society and IOP Publishing Ltd. All rights, including for text and data mining, AI training, and similar technologies, are reserved.

is actually a pure magnetic-type spin effect since the potentials $\{\Phi = 0, \mathcal{A} \neq 0\}$ have been chosen. For convenience, let us call the conventional SG experiment the magnetic-type SG (MTSG) effect. The MTSG effect not only reveals that the magnetic moments are quantized but also indicates an interesting physical phenomenon: as an internal degree of freedom, the spin can indeed affect the external motion of atoms (i.e., through the vector potential $\mathcal{A}$, or through the interaction $\boldsymbol{\mu}\cdot\mathcal{B}$ between the spin and the magnetic field). However, the MTSG effect is only half of the story of the whole family of SG effects. This naturally raises a scientific question: What type of spin effect arises if the potentials $\{\Phi \neq 0, \mathcal{A} = 0\}$ are considered? In this work, we advance the study of the SG effect. By considering the potentials $\{\Phi \neq 0, \mathcal{A} = 0\}$ in Dirac's equation, we present an extraordinary spin effect — the electric-type Stern–Gerlach (ETSG) effect. For simplicity, we choose the scalar potential as a one-dimensional potential barrier. After exactly solving Dirac's equation, we obtain the explicit forms of incident, reflected, and transmitted waves. The ETSG effect shows that the reflected and transmitted waves can exhibit notable spatial shifts, which depend on the spin direction and the incident angle of the wave. This electric-type spin effect has potential applications for separating Dirac particles (i.e., the incident waves) with different spin directions and for estimating the spin direction of Dirac particles.

2. Results

The potential barrier is given by[7]

$$V(x) = q\Phi = \begin{cases} V_0, & x > 0, \\ 0, & x \leq 0, \end{cases} \tag{2}$$

with $V_0 > 0$. By solving Dirac's equation, one can determine the incident, reflected, and transmitted waves. Due to wave-particle duality, these matter waves represent Dirac particles themselves. In Fig. 1, the reflecting interface is the yz-plane, point O is the incident point, and $|\Psi_{\rm in}\rangle$, $|\Psi_{\rm r}\rangle$, and $|\Psi_{\rm t}\rangle$ are, respectively, the incident, reflected, and transmitted waves. $\varphi_{\rm in}$, $\varphi_{\rm r}$, and $\varphi_{\rm t}$ are the corresponding incident, reflected, and transmitted angles. Similar to wave optics, after the incident wave arrives at point O, reflection and transmission phenomena generally occur. However, due to the existence of "spin" for Dirac particles, there are spatial shifts deviating from point O for the reflected and transmitted waves, denoted as $\Delta z_{\rm r}$ and $\Delta z_{\rm t}$.

In this work, we consider the incident finite-width wave $|\Psi_{\rm in}\rangle$. For simplicity, we assume the momentum $p_y = 0$ (i.e., the incident plane is just the xz-plane as shown in Fig. 1), and the effective wavefront area of the incident wave has finite dimensions along the z-axis and infinite dimensions along the y-axis. $|\Psi_{\rm in}\rangle$ can be represented as the superposition of infinite-width incident waves, namely,

$$|\Psi_{\rm in}\rangle = \int {\rm d}k_z \begin{pmatrix} (\mathcal{E}+mc^2)\,|\chi\rangle \\ c\hbar(\boldsymbol{\sigma}\cdot\boldsymbol{k})\,|\chi\rangle \end{pmatrix} \frac{{\rm e}^{{\rm i}\left[(k_x x + k_z z) - \frac{1}{\hbar}\mathcal{E}t\right]}}{\sqrt{2\mathcal{E}(\mathcal{E}+mc^2)}}, \tag{3}$$

where $\boldsymbol{k} = \boldsymbol{p}/\hbar = (k_x, 0, k_z)$, and $\mathcal{E} = +\sqrt{\boldsymbol{p}^2c^2 + m^2c^4}$ corresponds to the positive energy of Dirac particles. This ensures that the energy of Dirac particles remains positive during their motion. The state $|\chi\rangle = \begin{pmatrix} \cos\frac{\theta}{2} \\ \sin\frac{\theta}{2}\,{\rm e}^{{\rm i}\phi} \end{pmatrix}$ indicates the spin direction $\boldsymbol{\tau} = (\tau_x, \tau_y, \tau_z)$ of the incident wave $|\Psi_{\rm in}\rangle$, with $|\chi\rangle\langle\chi| = (\mathbb{1} + \boldsymbol{\sigma}\cdot\boldsymbol{\tau})/2$ and $\mathbb{1}$ being the 2×2 unit matrix.[8] Generally, $|\chi\rangle$ is independent of $\boldsymbol{k}$.

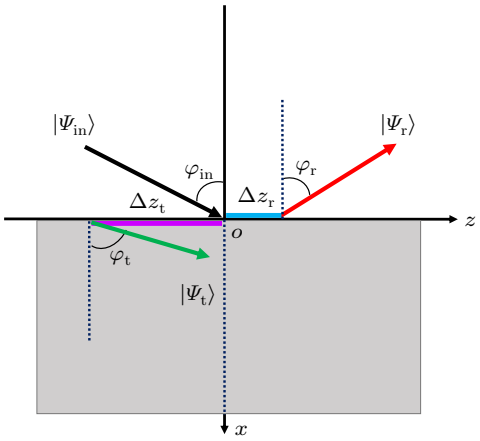


Fig. 1. Illustration of the ETSG effect. $|\Psi_{\rm in}\rangle$ is the incident wave (solid black arrow), $|\Psi_{\rm r}\rangle$ is the reflected wave (solid red arrow), and $|\Psi_{\rm t}\rangle$ is the transmitted wave (solid green arrow). $\varphi_{\rm in}$ is the incident angle, $\varphi_{\rm r}$ is the reflected angle, and $\varphi_{\rm t}$ is the transmitted angle. The reflected wave has a spatial shift $\Delta z_{\rm r}$ (solid blue line), and the transmitted wave has a spatial shift $\Delta z_{\rm t}$ (solid purple line), which are on the order of the Compton wavelength. The shifts can be positive or negative, depending on the spin direction and the incident angle of the wave. The ETSG effect is a purely relativistic effect caused by spin, which vanishes in the non-relativistic limit.

We assume that when $x = 0$, $|\Psi_{\rm in}\rangle$ approximately satisfies the following relation:

$$|\Psi_{\rm in}\rangle\,(0,z) = \begin{cases} \begin{pmatrix} (\mathcal{E}+mc^2)\,|\chi\rangle \\ c\hbar(\boldsymbol{\sigma}\cdot\boldsymbol{k}_0)\,|\chi\rangle \end{pmatrix} \frac{{\rm e}^{{\rm i}\left(k_{z_0}z - \frac{1}{\hbar}\mathcal{E}t\right)}}{\sqrt{2\mathcal{E}(\mathcal{E}+mc^2)}}, & |z| \leq a, \\ 0, & |z| > a, \end{cases}$$

where $\boldsymbol{k}_0 = (k_{x_0}, 0, k_{z_0})$ can be regarded as the average momentum of the incident finite-width wave, and $2a$ is the beam width. Accordingly, only the components whose k_z are very close to the average momentum k_{z_0} of the incident wave need to be considered.

We designate the momenta of the reflected and transmitted waves as $\boldsymbol{p}_{\rm r} = \hbar\boldsymbol{k}_{\rm r} = \hbar(-k_x, 0, k_z)$ and $\boldsymbol{p}_{\rm t} = \hbar\boldsymbol{k}_{\rm t} = \hbar(k'_x, 0, k_z)$, respectively. They satisfy the energy–momentum relations $\mathcal{E}^2 = \boldsymbol{p}_{\rm r}^2c^2 + m^2c^4$ and $(\mathcal{E} - V_0)^2 = \boldsymbol{p}_{\rm t}^2c^2 + m^2c^4$. Then, in the y-basis $\{|\uparrow\rangle_y, |\downarrow\rangle_y\}$, the finite-width reflected and transmitted waves read

$$|\Psi_{\rm r}\rangle = \int {\rm d}k_z \left\{ |A'|\,{\rm e}^{{\rm i}\theta_a} \begin{pmatrix} (\mathcal{E}+mc^2)|\uparrow\rangle_y \\ c\hbar(\boldsymbol{\sigma}\cdot\boldsymbol{k}_{\rm r})|\uparrow\rangle_y \end{pmatrix} + |B'|\,{\rm e}^{{\rm i}\theta_b} \begin{pmatrix} (\mathcal{E}+mc^2)|\downarrow\rangle_y \\ c\hbar(\boldsymbol{\sigma}\cdot\boldsymbol{k}_{\rm r})|\downarrow\rangle_y \end{pmatrix} \right\} \frac{{\rm e}^{{\rm i}\left[(-k_x x+k_z z)-\frac{1}{\hbar}\mathcal{E}t\right]}}{\sqrt{2\mathcal{E}(\mathcal{E}+mc^2)}}, \tag{4a}$$

$$|\Psi_{\rm t}\rangle = \int {\rm d}k_z \left\{ |C'|\,{\rm e}^{{\rm i}\theta_c} \begin{pmatrix} (\mathcal{E}+mc^2)|\uparrow\rangle_y \\ c\hbar(\boldsymbol{\sigma}\cdot\boldsymbol{k}_{\rm t})|\uparrow\rangle_y \end{pmatrix} + |D'|\,{\rm e}^{{\rm i}\theta_d} \begin{pmatrix} (\mathcal{E}+mc^2)|\downarrow\rangle_y \\ c\hbar(\boldsymbol{\sigma}\cdot\boldsymbol{k}_{\rm t})|\downarrow\rangle_y \end{pmatrix} \right\} \frac{{\rm e}^{{\rm i}\left[(k'_x x+k_z z)-\frac{1}{\hbar}\mathcal{E}t\right]}}{\sqrt{2(\mathcal{E}-V_0)(\mathcal{E}-V_0+mc^2)}}, \tag{4b}$$

where A', B', C', and D' are superposition coefficients. The states $|\uparrow\rangle_y$ and $|\downarrow\rangle_y$ correspond to the spin directions $\boldsymbol{\tau} = (0,1,0)$ and $(0,-1,0)$, respectively. In the y-basis, one has the simple relations $\theta_b = -\theta_a$, $\theta_d = -\theta_c$, and

$$\tan\theta_a = -\frac{2k_x k_z(n-1)}{k_x^2 - k_z^2(n-1)^2 - k_x'^2 n^2},$$
$$\tan\theta_c = -\frac{k_z(1-n)}{k_x + nk'_x}, \tag{5}$$

with $n = \frac{\mathcal{E}+mc^2}{\mathcal{E}-V_0+mc^2}$ representing the "refractive index". Similar to the case of the incident wave, only the components whose k_z are very close to the average momentum k_{z_0} of the reflected and transmitted waves need to be considered. This allows us to apply the stationary phase method,[9] which has been used for calculating various Goos-Hänchen (GH) shifts in wave optics and quantum mechanics.[10–20]

According to the stationary phase method, the spatial shift is defined by $\Delta z = -\partial\theta/\partial k_z$. Then, the spatial shifts of the reflected and transmitted waves are given by

$$\Delta z_{\rm r} = -\frac{1}{|A'|^2+|B'|^2}\left(|A'|^2\frac{\partial\theta_a}{\partial k_z} + |B'|^2\frac{\partial\theta_b}{\partial k_z}\right) = \frac{\hbar}{mc}\times\tau_y\frac{\sqrt{1-\mu_{\rm E}}}{\sqrt{1+\mu_{\rm E}}}\times\frac{\mu_{\rm E}\cos\varphi}{\sin^2\varphi+\mu_{\rm E}^2\cos^2\varphi}\left(\tan^2\varphi-\mu_{\rm E}\right), \tag{6a}$$

$$\Delta z_{\rm t} = -\frac{\hbar}{mc}\times\frac{\tau_y}{2\mu_{\rm V}}\times\frac{\dfrac{\sqrt{1-\mu_{\rm E}}}{\sqrt{1+\mu_{\rm E}}}\dfrac{1}{\cos\varphi}+\dfrac{\dfrac{1}{\mu_{\rm E}}-\dfrac{1}{\mu_{\rm V}}-1}{\sqrt{\dfrac{1}{\mu_{\rm V}}\left(\dfrac{1}{\mu_{\rm V}}-\dfrac{2}{\mu_{\rm E}}\right)+\left(\dfrac{1}{\mu_{\rm E}^2}-1\right)\cos^2\varphi}}}{\sqrt{\dfrac{1}{\mu_{\rm E}^2}-1}\times\cos\varphi\times\left[\sqrt{\dfrac{1}{\mu_{\rm E}^2}-1}\times\cos\varphi+\sqrt{\dfrac{1}{\mu_{\rm V}}\left(\dfrac{1}{\mu_{\rm V}}-\dfrac{2}{\mu_{\rm E}}\right)+\left(\dfrac{1}{\mu_{\rm E}^2}-1\right)\cos^2\varphi}\right]-\dfrac{1}{\mu_{\rm E}\mu_{\rm V}}}, \tag{6b}$$

where $\mu_{\rm E} = mc^2/\mathcal{E}$, $\mu_{\rm V} = mc^2/V_0$, $\tau_y = \boldsymbol{\tau}\cdot\boldsymbol{e}_y$ is the y-component of spin direction of the incident wave, and φ is the incident angle satisfying $\tan\varphi = k_z/k_x$ and $\varphi\in[0,\pi/2)$.

Remark 1 For the incident angle, there are two critical angles, denoted by $\varphi_{\rm cr1}$ and $\varphi_{\rm cr2}$, respectively. $\varphi_{\rm cr1}$ is the critical angle for total reflection, which is a common phenomenon for waves. Namely, if the incident angle $\varphi\geq\varphi_{\rm cr1}$, total reflection occurs (i.e., the transmission vanishes). The first angle $\varphi_{\rm cr1}$ can be determined from the condition that the transmission coefficient $\mathcal{T}=0$, yielding

$$\varphi_{\rm cr1} = \arcsin\left(\sqrt{\frac{(\mathcal{E}-V_0)^2-m^2c^4}{\mathcal{E}^2-m^2c^4}}\right).$$

Here, the energy region $\mathcal{E}-V_0+mc^2>0$ (or $n>0$) is considered to avoid Klein's paradox[21] in relativistic quantum mechanics. The second angle $\varphi_{\rm cr2}$ is determined by $\Delta z_{\rm r}=0$, i.e.,

$$\varphi_{\rm cr2} = \arctan\sqrt{\frac{mc^2}{\mathcal{E}}}.$$

In the literature, GH shifts for optical and matter waves occur in the region $\varphi\geq\varphi_{\rm cr1}$. However, the ETSG effect is an extraordinary spin effect (see the explanation in Table 1 below). To distinguish the ETSG effect from the GH effect, we restrict our study to the region $\varphi\in[\varphi_{\rm cr2},\varphi_{\rm cr1}]$.

Remark 2 From Eqs. (6a) and (6b), one finds that the spatial shifts $\Delta z_{\rm r}$ and $\Delta z_{\rm t}$ are both on the order of the Compton wavelength $\lambda = h/(mc)$, with $h = 2\pi\hbar$.

Table 1. The behaviors of $\Delta z_{\rm r}$ and $\Delta z_{\rm t}$ with respect to φ and τ_y. If the spin direction is reversed, i.e., $\boldsymbol{\tau}\mapsto-\boldsymbol{\tau}$, the signs of the spatial shifts are also reversed, indicating that the ETSG effect is indeed a spin-dependent effect.

Shift	φ	$0<\tau_y\leq1$	$\tau_y=0$	$-1\leq\tau_y<0$
$\Delta z_{\rm r}$	$\varphi\in[0,\varphi_{\rm cr2})$	$-$	0	$+$
	$\varphi=\varphi_{\rm cr2}$	0	0	0
	$\varphi\in(\varphi_{\rm cr2},\varphi_{\rm cr1})$	$+$	0	$-$
$\Delta z_{\rm t}$	$\varphi\in[0,\varphi_{\rm cr1})$	$-$	0	$+$

Remark 3 Under the non-relativistic approximation, one has $|\boldsymbol{p}|\approx0$. This yields $\mathcal{E}-mc^2\approx0$, $V_0\approx\frac{\boldsymbol{p}^2}{2m}\approx\mathcal{E}-mc^2\approx0$, thus $\Delta z_{\rm r}$ (and $\Delta z_{\rm t}$) $\propto\sqrt{\mathcal{E}-mc^2}\approx0$. This implies that, unlike the MTSG effect, the ETSG effect vanishes in the non-relativistic limit. Therefore, the spatial shifts for the reflected and transmitted waves are purely relativistic effects caused by spin, which explains why the ETSG effect has not been observed in non-relativistic quantum mechanics.

Remark 4 If the momentum p_y is nonzero, the incident

wave must satisfy the following relation:

$$|\Psi_{\rm in}\rangle(0,y,z) = \begin{cases} \begin{pmatrix} (\mathcal{E}+mc^2)|\chi\rangle \\ c\hbar(\boldsymbol{\sigma}\cdot\boldsymbol{k}_0)|\chi\rangle \end{pmatrix} \frac{e^{i\left[k_{y0}y+k_{z0}z-\frac{1}{\hbar}\mathcal{E}t\right]}}{\sqrt{2\mathcal{E}(\mathcal{E}+mc^2)}}, & |y|\le a,\ |z|\le b, \\ 0, & \text{otherwise}, \end{cases} \tag{7}$$

where $2a$ and $2b$ are the beam widths along the y-axis and z-axis, respectively. The reflected and transmitted waves are similar to Eq. (4), with an additional term $k_y y$ in the exponential. According to $\Delta y = -\hbar\frac{\partial\theta}{\partial p_y}$ and $\Delta z = -\hbar\frac{\partial\theta}{\partial p_z}$, the same method as above can be used to obtain Δy and Δz for the reflected and transmitted waves.

$$\Delta\boldsymbol{l}_{\rm r} = \Delta y_{\rm r}\boldsymbol{e}_y + \Delta z_{\rm r}\boldsymbol{e}_z = \frac{\hbar^2c^2}{k_x(\mathcal{E}+mc^2)^2[\mathcal{E}^2-c^2\hbar^2k_x^2]} \times\left\{\mathcal{E}(\mathcal{E}+mc^2)[(\boldsymbol{\tau}\times\boldsymbol{k})\cdot\boldsymbol{e}_x]\boldsymbol{\eta}+k_x^2mc^2(\mathcal{E}+mc^2)(\boldsymbol{\tau}\times\boldsymbol{e}_x)+c^2\hbar^2k_x^2(\boldsymbol{k}\cdot\boldsymbol{\tau})(\boldsymbol{k}\times\boldsymbol{e}_x)\right\}, \tag{8a}$$

$$\Delta\boldsymbol{l}_{\rm t} = \Delta y_{\rm t}\boldsymbol{e}_y + \Delta z_{\rm t}\boldsymbol{e}_z = -\kappa_3(n-1)\left\{\kappa_1\left[(\boldsymbol{\tau}\times\boldsymbol{k})\cdot\boldsymbol{e}_x\right]\boldsymbol{\eta}-\kappa_2(\boldsymbol{\tau}\times\boldsymbol{e}_x)+(n-1)(\boldsymbol{\tau}\cdot\boldsymbol{e}_x)(\boldsymbol{e}_x\times\boldsymbol{k})\right\}, \tag{8b}$$

with $\boldsymbol{\eta} = k_y\boldsymbol{e}_y + k_z\boldsymbol{e}_z$, $\kappa_1 = \frac{1}{k_x}+\frac{n}{k_x'}$, $\kappa_2 = k_x + nk_x'$, $\kappa_3 = \frac{1}{(k_x+nk_x')^2+(n-1)^2(k_y^2+k_z^2)}$. One may observe that when the spin direction is reversed, i.e., $\boldsymbol{\tau}\mapsto-\boldsymbol{\tau}$, the spatial shifts $\Delta\boldsymbol{l}_{\rm r}$ and $\Delta\boldsymbol{l}_{\rm t}$ are also reversed. The scalar potential Eq. (2) corresponds to an electric field $\mathbb{E}$ along the x-axis; if one denotes $\boldsymbol{e}_x = \mathbb{E}/|\mathbb{E}|$, it is clear that the spatial shifts are related to the interaction between spin and the electric field. When $k_y = 0$, Eqs. (8a) and (8b) reduce to Eqs. (6a) and (6b).

3. Application

In Table 1, we have demonstrated the behaviors of the spatial shifts for the reflected and transmitted waves. One finds that the shift $\Delta z_{\rm r}$ can be positive, zero, or negative, depending on the choices of τ_y and the incident angle φ, while the shift $\Delta z_{\rm t}$ can be positive, zero, or negative, depending solely on the choice of τ_y. In Fig. 1, we have illustrated the case of $\Delta z_{\rm r} > 0$ and $\Delta z_{\rm t} < 0$, which corresponds to $0 < \tau_y \le 1$ and $\varphi \in (\varphi_{\rm cr2}, \varphi_{\rm cr1})$. Based on these findings, we can propose the following potential applications:

(i) Separating Dirac particles with different spin directions. The spin direction of a Dirac particle is encoded in the incident wave $|\Psi_{\rm in}\rangle$ (or in the state $|\chi\rangle$). In Fig. 2, we illustrate the spin direction $\boldsymbol{\tau}$ on the Bloch sphere.[8] For simplicity, we refer to the xz-plane as the "equatorial plane," the hemispherical surface above the xz-plane as the "northern hemisphere," the hemispherical surface below the xz-plane as the "southern hemisphere," the intersection of the positive y-axis with the sphere as the north pole, and the intersection of the negative y-axis with the sphere as the south pole. Then, the results in Table 1 can be used to separate Dirac particles with different spin directions. The procedure is as follows: for a beam of incident Dirac particles, take the incident angle as $\varphi \in [0, \varphi_{\rm cr2})$. After reflection, particles with spin directions in the "northern hemisphere" will have negative shifts $\Delta z_{\rm r}$, those in the "southern hemisphere" will have positive shifts $\Delta z_{\rm r}$, and those in the "equatorial plane" will have no shift, thereby realizing the separation of Dirac particles with different spin directions via the ETSG effect.

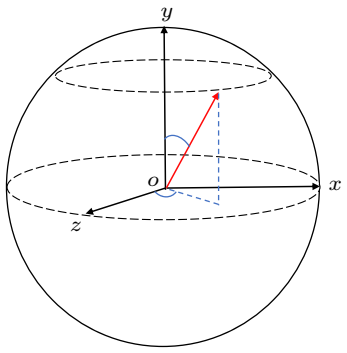


Fig. 2. Illustration of the spin direction of $|\Psi_{\rm in}\rangle$ on the Bloch sphere. $\boldsymbol{\tau} = (\tau_x, \tau_y, \tau_z)$ represents the spin direction (red solid arrow).

(ii) Estimating the spin direction of Dirac particles. Conversely, one can use the results in Table 1 to estimate the spin direction of an incident Dirac particle. The procedure is as follows: take the incident angle as $\varphi \in [0, \varphi_{\rm cr2})$. If a negative shift $\Delta z_{\rm r}$ occurs, the spin direction of the Dirac particle lies in the "northern hemisphere"; if a positive shift occurs, it lies in the "southern hemisphere"; if no shift occurs, it is located in the "equatorial plane." In this way, the ETSG effect enables the estimation of spin directions of Dirac particles.

4. Some theoretical data

Here we provide some theoretical data that may assist experimental scientists in performing possible experiments. Let us choose the parameters $\mu_{\rm E} = 1/3$, $\mu_{\rm V} = 4$, and $\tau_y \approx 0.92$, which correspond to $\mathcal{E}$ and V_0 on the order of MeV. These parameters yield two critical angles: $\varphi_{\rm cr1} \approx 64.92^\circ$ and $\varphi_{\rm cr2} = 30^\circ$. In Table 2, we list the variations of the reflected angle $\varphi_{\rm r}$, the transmitted angle $\varphi_{\rm t}$, and the spatial shifts $\Delta z_{\rm r}$ and $\Delta z_{\rm t}$ as the incident angle $\varphi_{\rm in}$ varies from 0° to the critical angle $\varphi_{\rm cr1}$. With current quantum technologies in precision measurement or interferometry, it may be possible to observe the ETSG effect in the laboratory.

Table 2. Variations of the reflected angle $\varphi_{\rm r}$, the transmitted angle $\varphi_{\rm t}$, and the spatial shifts $\Delta z_{\rm r}$ and $\Delta z_{\rm t}$ as the incident angle φ varies from 0° to the critical angle $\varphi_{\rm cr1} \approx 64.92°$. Here, $\mu_{\rm E} = 1/3$, $\mu_{\rm V} = 4$, and $\tau_y \approx 0.92$; $\varphi_{\rm r} = \varphi_{\rm in}$, and $\varphi_{\rm t}$ satisfies $\tan\varphi_{\rm t} = k_z/k_x'$ with $k_x'^2 = \left[(\mathcal{E}-V_0)^2 - \left(\hbar^2 k_z^2 c^2 + m^2 c^4\right)\right]/(\hbar c)^2$. The units of $\Delta z_{\rm r}$ and $\Delta z_{\rm t}$ are taken as $h/(mc)$.

$\varphi_{\rm in}$	0°	2°	4°	6°	8°	10°	12°	14°	16°	18°	20°	22°
$\varphi_{\rm r}$	0°	2°	4°	6°	8°	10°	12°	14°	16°	18°	20°	22°
$\varphi_{\rm t}$	0°	2.21°	4.42°	6.62°	8.84°	11.05°	13.27°	15.49°	17.72°	19.95°	22.19°	24.43°
$\Delta z_{\rm r}$	−0.1035	−0.1021	−0.0980	−0.0916	−0.0835	−0.0745	−0.0650	−0.0556	−0.0466	−0.0381	−0.0302	−0.0231
$\Delta z_{\rm t}$	−0.0302	−0.0302	−0.0304	−0.0308	−0.0312	−0.0318	−0.0326	−0.0335	−0.0347	−0.0360	−0.0376	−0.0394
$\varphi_{\rm in}$	24°	26°	28°	30°	32°	34°	36°	38°	40°	42°	44°	46°
$\varphi_{\rm r}$	24°	26°	28°	30°	32°	34°	36°	38°	40°	42°	44°	46°
$\varphi_{\rm t}$	26.68°	28.95°	31.22°	33.51°	35.81°	38.13°	40.46°	42.82°	45.21°	47.63°	50.08°	52.58°
$\Delta z_{\rm r}$	−0.0165	−0.0105	−0.0050	0	0.0046	0.0089	0.0130	0.0168	0.0205	0.0241	0.0275	0.0310
$\Delta z_{\rm t}$	−0.0416	−0.0441	−0.0470	−0.0505	−0.0546	−0.0595	−0.0653	−0.0723	0.0809	−0.0914	−0.1046	−0.1214
$\varphi_{\rm in}$	48°	50°	52°	54°	56°	58°	59°	60°	61°	62°	63°	64°
$\varphi_{\rm r}$	48°	50°	52°	54°	56°	58°	59°	60°	61°	62°	63°	64°
$\varphi_{\rm t}$	55.14°	57.76°	60.46°	63.28°	66.25°	69.44°	71.16°	72.98°	74.94°	77.13°	79.66°	82.91°
$\Delta z_{\rm r}$	0.0345	0.0381	0.0418	0.0457	0.0498	0.0543	0.0567	0.0592	0.0617	0.0646	0.0675	0.0706
$\Delta z_{\rm t}$	−0.1433	−0.1725	−0.2132	−0.2722	−0.3639	−0.5207	−0.6475	−0.8373	−1.1481	−1.7366	−3.2110	−11.6888

5. Discussion and conclusion

In summary, we have presented an extraordinary spin effect, i.e., the ETSG effect, by exactly solving Dirac's equation with a vector potential $\mathcal{A} = 0$ and a simple scalar potential Φ given in Eq. (2). Our work constitutes a nontrivial generalization of the conventional SG effect from magnetic-type to electric-type, thereby improving and complementing the study of the SG effect. This work also completes the other half of the SG effect, thus enriching the family of SG effects. Unlike the MTSG effect, the ETSG effect vanishes in the non-relativistic limit, meaning that the spatial shifts for the reflected and transmitted waves are pure relativistic effects caused by spin, which deepens the understanding of the concept of *spin*. We anticipate that the ETSG effect can be observed in the near future. If realized experimentally, it could provide a significant technique for separating Dirac particles with different spin directions as well as for estimating their spin orientations.

We conclude with several discussions:

(i) Although the ETSG effect resembles a GH-like shift, they are fundamentally different. The GH shift occurs only in the region of total reflection and does not require the notion of "spin," whereas the ETSG effect occurs in the region of non-total reflection and crucially depends on spin. Investigating Dirac's equation for $\varphi \in [\varphi_{\rm cr1}, \pi/2)$ is expected to reveal a mixture of ETSG and GH effects, which we plan to study in future work.[22]

(ii) In the present study, we have considered a specific case and neglected possible shifts along the y-axis and the influence of p_y. A more comprehensive analysis can be carried out for the general case with $p_y \neq 0$ and an incident wavefront of finite extent along both the z- and y-axes. In such cases, Imbert–Fedorov-like shifts are expected,[23–25] i.e., $\Delta\boldsymbol{l}_{\rm r} = \Delta y_{\rm r}\boldsymbol{e}_y + \Delta z_{\rm r}\boldsymbol{e}_z$ and $\Delta\boldsymbol{l}_{\rm t} = \Delta y_{\rm t}\boldsymbol{e}_y + \Delta z_{\rm t}\boldsymbol{e}_z$.

(iii) The potential barrier in Eq. (2) is a step-like model. Although in reality matter waves often propagate in continuous fields, this model provides insight into spatial shifts. To analyze continuous fields, one can approximate the field as a sequence of infinitesimal potential steps and compute spatial shifts interval by interval, thereby describing the propagation of matter waves.

For example, consider the linear potential

$$V(x) = q\Phi(x) = \begin{cases} -q\mathbb{E}_0 x > 0, & x > 0, \\ 0, & x \leq 0, \end{cases} \tag{9}$$

where $q = -e$ (with $e = |e| > 0$) is the electron charge, and $\Phi(x) = -\mathbb{E}_0 x$ is the scalar potential with $\mathbb{E}_0 > 0$. The corresponding electric field is $\mathbb{E} = -\boldsymbol{\nabla}\Phi(x) = \mathbb{E}_0\boldsymbol{e}_x$, a uniform field along the positive x-axis.

Solving Dirac's equation exactly for Eq. (9) is challenging. Alternatively, one can divide the space into infinitesimal intervals along the x-axis, each of width $\mathrm{d}x \to 0$. This method is valid when p_x is not too small. Assuming a plane matter wave passes through many infinitesimal-width barriers, the above approach can be applied to determine the spatial shifts in each interval.

For a single interval, the incident wave energy is $\mathcal{E}$ and the potential is $V_0 = -q\mathbb{E}_0\mathrm{d}x \approx 0$, yielding $(n-1) \to 0$ and $k_x' \approx k_x$. This gives a transmission coefficient $\mathcal{T} = 1$ and reflection coefficient $\mathcal{R} = 0$, i.e., no reflected wave. The spatial shift of the transmitted wave is then

$$\Delta\boldsymbol{l}_{\rm t} \approx \frac{q\,\mathrm{d}x}{2k_x^3(\mathcal{E}+mc^2)}\left\{[(\boldsymbol{\tau}\times\boldsymbol{k})\cdot\mathbb{E}]\boldsymbol{\eta} - k_x^2(\boldsymbol{\tau}\times\mathbb{E})\right\}, \tag{10}$$

with $\boldsymbol{\eta} = (0, k_y, k_z) = \boldsymbol{k} - k_x(\mathbb{E}/\mathbb{E}_0)$ and $k_x = \boldsymbol{k}\cdot(\mathbb{E}/\mathbb{E}_0)$. For subsequent intervals, $\mathcal{E} \to \mathcal{E} + q\mathbb{E}_0\mathrm{d}x$, and corresponding spatial shifts can be computed iteratively to describe wave propagation. This approach generalizes to any one-dimensional continuous field. Equation (10) confirms that the ETSG effect arises from spin–electric field interaction; for instance,

$(\boldsymbol{\tau} \times \boldsymbol{k}) \cdot \mathbb{E}$ represents Rashba-like spin–orbit coupling,[26] which can induce the spin Hall effect in an electric field.[27–29] Investigating the connection between the ETSG effect and the spin Hall effect is an interesting direction for future work.

Acknowledgments

This project is supported by the Quantum Science and Technology-National Science and Technology Major Project of China (Grant No. 2024ZD0301000) and the National Natural Science Foundation of China (Grant No. 12275136).

References

[1] Greiner W 2001 *Quantum Mechanics: An Introduction* (Berlin: Springer) pp. 329–353
[2] Uhlenbeck G E and Goudsmit S 1925 *Nat. Wiss.* **13** 953 (in German)
[3] Uhlenbeck G E and Goudsmit S 1926 *Nature* **117** 264
[4] Dirac P A M 1928 *Proc. R. Soc. Lond. A* **117** 610
[5] Greiner W 2000 *Relativistic Quantum Mechanics. Wave Equations* (Berlin : Springer) p. 99
[6] Pauli Jr W 1927 *Z. Phys.* **43** 601 (in German)
[7] Flügge S 1999 *Practical Quantum Mechanics* (Berlin: Springer) p. 337
[8] Nielsen M A and Chuang I L 2010 *Quantum Computation and Quantum Information: 10th Anniversary Edition* (Cambridge: Cambridge University Press) pp. 171–247
[9] Artmann K 1948 *Ann. Phys.* **437** 87 (in German)
[10] Goos F and Hänchen H 1947 *Ann. Phys.* **436** 333 (in German)
[11] Mâaza M and Pardo B 1997 *Opt. Commun.* **142** 84
[12] Ignatovich V K 2004 *Phys. Lett. A* **322** 36
[13] Beenakker C W J, Sepkhanov R A, Akhmerov A R and Tworzydlo J 2009 *Phys. Rev. Lett.* **102** 146804
[14] de Haan V O, Plomp J, Rekveldt T M, Kraan W H, van Well A A, Dalgliesh R M and Langridge S 2010 *Phys. Rev. Lett.* **104** 010401
[15] Cheng M 2012 *Eur. Phys. J. B* **85** 89
[16] Zhou L, Qin J L, Lan Z, Dong G and Zhang W 2015 *Phys. Rev. A* **91** 031603(R)
[17] Huamán A and Usaj G 2019 *Phys. Rev. A* **100** 033409
[18] Ban Y and Chen X 2023 *Phys. Rev. A* **108** 042218
[19] Zhou J L, Zhang Z X, Fan X Y and Chen J L 2024 *Phys. Rev. A* **110** 042202
[20] Xiang H and Zhai F 2024 *Phys. Rev. B* **109** 035432
[21] Krekora P, Su Q and Grobe R 2004 *Phys. Rev. Lett.* **92** 040406
[22] Hu M J, Miao H X and Zhang Y S 2024 *Chin. Phys. B* **33** 020303
[23] Fedorov F I 2013 *J. Opt.* **15** 014002
[24] Imbert C 1972 *Phys. Rev. D* **5** 787
[25] Li C F 2007 *Phys. Rev. A* **76** 013811
[26] Manchon A, Koo H C, Nitta J, Frolov S M and Duine R A 2015 *Nature Mater.* **14** 871
[27] Hirsch J E 1999 *Phys. Rev. Lett.* **83** 1834
[28] Sinova J, Culcer D, Niu Q, Sinitsyn N A, Jungwirth T and MacDonald A H 2004 *Phys. Rev. Lett.* **92** 126603
[29] Nagaosa N, Sinova J, Onoda S, MacDonald A H and Ong N P 2010 *Rev. Mod. Phys.* **82** 1539